

Stretching of polymers around the Kolmogorov scale in a turbulent shear flow

Jahanshah Davoudi*¹ and Jörg Schumacher†¹

¹*Department of Physics, Philipps University Marburg, D-35032 Marburg, Germany*

(Dated: July 9, 2018)

We present numerical studies of stretching of Hookean dumbbells in a turbulent Navier-Stokes flow with a linear mean profile, $\langle u_x \rangle = Sy$. In addition to the turbulence features beyond the viscous Kolmogorov scale η , the dynamics at the equilibrium extension of the dumbbells significantly below η is well resolved. The variation of the constant shear rate S causes a change of the turbulent velocity fluctuations on all scales and thus of the intensity of local stretching rate of the advecting flow. The latter is measured by the maximum Lyapunov exponent λ_1 which is found to increase as $\lambda_1 \sim S^{3/2}$, in agreement with a dimensional argument. The ensemble of up to 2×10^6 passively advected dumbbells is advanced by Brownian dynamics simulations in combination with a pseudospectral integration for the turbulent shear flow. Anisotropy of stretching is quantified by the statistics of the azimuthal angle ϕ which measures the alignment with the mean flow axis in the x - y shear plane, and the polar angle θ which determines the orientation with respect to the shear plane. The asymmetry of the probability density function (PDF) of ϕ increases with growing shear rate S . Furthermore, the PDF becomes increasingly peaked around mean flow direction ($\phi = 0$). In contrast, the PDF of the polar angle θ is symmetric and less sensitive to changes of S .

PACS numbers: 47.27.ek, 83.10.Mj, 83.80.Rs

I. INTRODUCTION

When a few parts per million in weight of long-chained polymers are added to a turbulent fluid its properties change drastically and a significant reduction of turbulent drag is observed (see e.g. Refs. 1 and 2 for reviews). Although the phenomenon is known from pipe flow experiments for almost 60 years [3] a complete understanding is still lacking. It is observed in wall-bounded flows [4, 5, 6] as well as in bulk turbulence.[7, 8] The macroscopic drag reduction seems to go in line with a microscopic transition of the macromolecules from a preferentially coiled near-the-equilibrium to a stretched non-equilibrium state. The relation of the polymer dynamics at small scales to the flow statistics at larger scales is therefore essential for solving the drag reduction problem.[8, 9]

The dynamics of single long polymer chains in simple and partly steady flows is already quite complicated and rich with respect to conformational variety. This was demonstrated in experiments and Brownian dynamics simulations. [10, 11, 12, 13, 14] Only recently, a more complex situation was investigated – the stretching of polymer chains in random isotropic and random linear shear flows – by means of experiments in the so-called elastic turbulence limit.[15, 16] Analytic solutions are possible for the kinematic stretching of polymers in isotropic and white-in-time Kraichnan flow.[17, 18, 19, 20] The polymer chain is there described as two beads that are connected by a spring. The model is known as the mesoscopic dumbbell model and the entropic spring force follows either a linear Hookean or a nonlinear law. The latter captures the finite extensibility of the polymers.[21] Qualitatively new effects can be observed in a shear flow such as the tumbling, a flipping of the chain in the plane that is spanned by the shear flow.[11, 22] Analytical predictions for the tumbling statistics of dumbbells are possible when the isotropic Kraichnan flow is superposed with a linear shear flow at a very large shear rate.[23] The dynamics of the angular degrees of freedom can then be simplified significantly because the large shear aligns the dumbbells preferentially with the mean flow direction.

Although these studies give us a lot of helpful insights about the statistics of the extension and orientation of the polymer chains, the situation in a turbulent Navier-Stokes fluid is more complex. The flow structures are correlated in space *and* time and it can be expected that they cause significant differences in the stretching history of a chain while moving through the flow. Furthermore, turbulent fluctuations and the large scale shear are intimately coupled to each other. In other words, one cannot consider them as independently adjustable parameters. An increase of the shear rate S will change the Reynolds number of the flow and more importantly the ratio and magnitude of the turbulent velocity fluctuations $\langle u_i^2 \rangle$ with $i = x, y, z$ (see Refs. 24 and 25). For example, the presence of shear causes the generation of streamwise streaks, that enlarge the fluctuations in the streamwise direction.[26] As a consequence, we find that the maximum stretching rate grows with respect to S faster as recently predicted.[23]

* Present address: International Centre for Theoretical Physics, 34014 Trieste, Italy

† Present address: Department of Mechanical Engineering, Ilmenau University of Technology, D-98684 Ilmenau, Germany

The present work consists of two parts. The first part will focus on the statistics of the flow itself, at scales below and above the viscous Kolmogorov scale, $\eta = \frac{\nu^{3/4}}{\langle \epsilon \rangle^{1/4}}$, with ν being the kinematic viscosity and $\langle \epsilon \rangle$ the mean energy dissipation rate of the flow. We consider a simple turbulent shear flow with a linear mean profile which allows for studying the effects of shear on Lagrangian stretching rates. This in turn will reveal a different regime of polymer stretching in comparison with an analytic model of Chertkov *et al.*[23] The second part presents studies of the kinematics of polymer stretching in such flows. We will demonstrate that the interplay between the shear rate S and the Weissenberg number Wi is important for the stretching statistics. The dimensionless parameter Wi relates the local stretching rate of the flow to the relaxation rate of the polymers. Only the simplest mesoscopic polymer model, the Hookean dumbbell model [21], is discussed here. In the present study, the dumbbells do not react back on the shear flow. As it will turn out, turbulence is able to stop the stretching of the linear springs, but at a scale that is larger than the Kolmogorov scale of the flow.[27] Our approach intends to keep the polymer dynamics simple, but to take an advecting flow in its full turbulent complexity stemming from the Navier-Stokes equations.

In chapter II we present the dynamical equations for the flow and the dumbbells and discuss characteristic parameters. The dependence of local stretching rates on the shear rate is quantified in chapter III. The subsequent chapter summarizes our findings on the dumbbell dynamics where extension and angular statistics are discussed. Eventually, a summary and an outlook are given.

II. MODEL AND EQUATIONS

A. Advecting fluid

The Navier-Stokes equations for a three-dimensional incompressible fluid are solved by a pseudo-spectral method using a second-order predictor-corrector scheme for advancement in time.[28] The equations of motion are

$$\frac{\partial \mathbf{u}}{\partial t} + (\mathbf{u} \cdot \nabla) \mathbf{u} = -\nabla p + \nu \nabla^2 \mathbf{u} + \mathbf{f}, \quad (1)$$

$$\nabla \cdot \mathbf{u} = 0 \quad (2)$$

where \mathbf{u} is the (total) velocity field, p the kinematic pressure field, and \mathbf{f} the volume force density. The case without shear is solved in a three-dimensional box of side-length $L = 2\pi$ with periodic boundary conditions. The nearly homogeneous shear flow is modeled in a volume with free-slip boundary conditions in the shear direction y and periodic boundaries otherwise. Here the total velocity field follows by a Reynolds (de)composition as a linear mean part with the constant shear rate S and a turbulent fluctuating part

$$\mathbf{u} = \langle \mathbf{u} \rangle + \mathbf{v} = S y \mathbf{e}_x + \mathbf{v}. \quad (3)$$

The aspect ratio is $L_x : L_y : L_z = 2\pi : \pi : 2\pi$. The applied volume forcing is a combination of an isotropic forcing that injects energy at a fixed rate of $\epsilon_{in} = 0.1$ and a shear forcing. Consequently, $\langle \epsilon \rangle \equiv \epsilon_{in}$ for the statistically stationary case at $S = 0$. More details on the volume forcing and the numerical scheme can be found in Ref. 29. In Tab. 1, we summarize some statistical properties of the flows that were studied. Since we want to resolve eventually a range of scales below η , we are limited in the range of accessible Reynolds numbers although resolutions of up to $512 \times 257 \times 512$ grid points are used for the simulations.

B. Hookean dumbbells

The simplest description of polymer stretching can be accomplished by considering Hookean dumbbells. Their entropic elastic force is linearly dependent on the separation vector, $\mathbf{R} = \mathbf{x}_2 - \mathbf{x}_1$, that is spanned between both beads at positions $\mathbf{x}_2(t)$ and $\mathbf{x}_1(t)$, respectively. When taking into account the elastic entropic force, hydrodynamic Stokes drag, and thermal noise the evolution equation for \mathbf{R} reads [21, 30]

$$\dot{\mathbf{R}} = \Delta \mathbf{u} - \frac{\mathbf{R}}{2\tau} + \sqrt{\frac{R_0^2}{\tau}} \xi, \quad (4)$$

where $\Delta \mathbf{u} = \mathbf{u}(\mathbf{x}_2, t) - \mathbf{u}(\mathbf{x}_1, t)$ is the relative fluid velocity at the bead centers. The last term is the thermal Gaussian noise with the following properties

$$\langle \xi_i(t) \rangle = 0 \quad (5)$$

$$\langle \xi_i(t) \xi_j(t') \rangle = \delta_{ij} \delta(t - t') \quad (6)$$

run	1	2	3	4	5	6
S	0	$1/\pi$	$3/\pi$	$5/\pi$	$7/\pi$	$9/\pi$
ν	1/30	1/30	1/30	1/30	1/30	1/30
$\langle \epsilon \rangle$	0.100	0.113	0.285	0.845	2.268	5.179
R_λ	10.5	9.1	19.2	29.8	36.2	43.7
S^*	0	1.21	4.85	7.31	7.58	7.78
$S\tau_\eta$	0	0.17	0.33	0.32	0.27	0.23
T_{av}/T	20.5	25.1	18.9	21.0	112.8	70.7
$k_{max}\eta$	8.39	8.12	6.44	4.91	3.84	3.12

TABLE I: Parameters of the direct numerical simulations. S is the constant mean shear rate, ν the kinematic viscosity, $\langle \epsilon \rangle$ is the mean energy dissipation rate, $R_\lambda = \sqrt{5/(3\langle \epsilon \rangle \nu)} \langle v^2 \rangle$ is the Taylor microscale Reynolds number with the mean square of the turbulent velocity fluctuations $\langle v^2 \rangle$, and $S^* = S \langle v^2 \rangle / \langle \epsilon \rangle$ is the dimensionless shear parameter. The averaging time T_{av} is given in units of the large scale eddy turnover time $T = \langle v^2 \rangle / (2\langle \epsilon \rangle)$. The spectral resolution is indicated by $k_{max}\eta$ where $k_{max} = \sqrt{2}N/3$. All studies of the flow properties were done with $N = 128$.

with $i, j = x, y, z$. It prevents the extension of a dumbbell to shrink below its equilibrium length

$$R_0 = \sqrt{\frac{k_B T}{H}}, \quad (7)$$

with k_B being the Boltzmann constant, T the temperature, and H the spring constant of the Hookean spring. Equation (7) follows from the equipartition theorem. Time constant τ is the relaxation time of the polymers and is given for dumbbells as [21]

$$\tau = \frac{\zeta}{4H}, \quad (8)$$

where $\zeta = 6\pi\rho\nu a$ is the Stokes drag coefficient with fluid mass density ρ and bead radius a . We sketch in Fig. 1 the coordinate system that is used. Since we restrict our study to Hookean dumbbells, the effects of finite extension are not imposed by the potential. Therefore the extended dumbbells experience both the smooth and rough scales of the advecting flow during their time evolution. Consequently, the velocity difference $\Delta \mathbf{u}$ is *not* approximated by the linearization $(\mathbf{R} \cdot \nabla) \mathbf{u}$ in Eq. (4) as usually done. We solve the equations for the beads separately, but can reconstruct the full dynamics of \mathbf{R} afterwards. An ensemble of up to 2×10^6 dumbbells, i.e., 4×10^6 beads, is advanced by a weak second-order predictor-corrector scheme simultaneously with the flow equations.[30] Initially, their center of mass is seeded randomly in space with a uniform distribution and an initial extension of R_0 . All Lagrangian interpolations were done with a trilinear scheme since the velocity field is very well resolved as given by the spectral resolution factor $k_{max}\eta$ in Tab. 1.

C. Stretching rates

According to Eq. (4) the dynamics of dumbbells is subject to both, local stretching rate due to varying strain at small scales and restoring linear spring force. The separation vector between two fluid elements, $|\delta \mathbf{r}|$, evolves as

$$\frac{d}{dt} \delta r_j(t) = \sigma_{jk}(t) \delta r_k(t) \quad \text{for } j, k = x, y, z, \quad (9)$$

where $\sigma_{jk}(t)$ is the local stretching tensor along the Lagrangian trajectories. Consequently,

$$\delta r_j(t) = W_{jk}(t, 0) \delta r_k(0), \quad (10)$$

with the time-ordered exponential

$$W_{jk}(t, 0) = \mathcal{T}_+ \exp \left(\int_0^t \sigma_{jk}(\tau) d\tau \right), \quad (11)$$

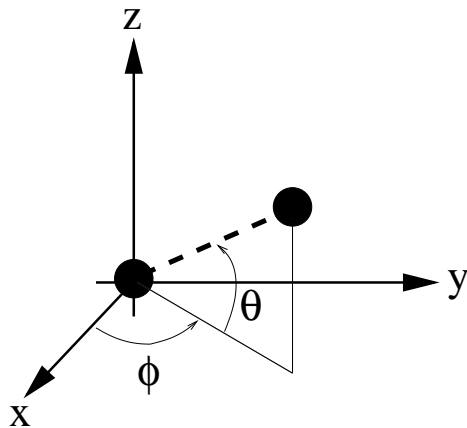


FIG. 1: Dumbbell coordinate system that is used throughout this text. It follows from the sketch that $R_x = R \cos \phi \cos \theta$, $R_y = R \sin \phi \cos \theta$, and $R_z = R \sin \theta$ where R is the distance between both beads. The notation differs from conventional spherical coordinates, but has the advantage of giving alignment with the outer mean flow for $\phi = \theta = 0$. ϕ is azimuthal angle and θ the polar angle.

where $\delta \mathbf{r}(0)$ is the initial separation vector. The local stretching and contraction rates are quantified by the Lyapunov exponents

$$\lambda_i = \lim_{t \rightarrow \infty} \frac{1}{t} \langle \log \left(\frac{|\delta \mathbf{r}^{(i)}(t)|}{|\delta \mathbf{r}^{(i)}(0)|} \right) \rangle_L, \quad (12)$$

with $i = 1, 2, 3$ for three dimensions and $\lambda_1 \geq \lambda_2 \geq \lambda_3$. [31, 32] The subscript L is an average over different realizations of the Lagrangian tracer tracks. The largest Lyapunov exponent, λ_1 , quantifies the growth of the norm of the separation vector $\delta \mathbf{r}$. The exponents are long-time averages of Lagrangian simulations following the algorithm by Benettin *et al.* [31]. Figure 2 illustrates that the convergence of the Lyapunov spectrum for a larger shear rate requires a long time series. A sufficient convergence is reached there after about 70 large eddy turnover times the latter of which is defined as $T = \langle v^2 \rangle / (2 \langle \epsilon \rangle)$. Clearly this procedure has to be done for each S value anew.

While the mean stretching time scale in a turbulent flow is given by the λ_1^{-1} , the beads relax back to their coiled equilibrium distance within times of the order of τ . The Weissenberg number which is defined as

$$Wi = \lambda_1 \tau, \quad (13)$$

is an appropriate measure for the competition of those mechanisms. For $Wi < 1/2$ the relaxation to equilibrium size is on average faster than stretching by the flow. Polymers are preferentially in a coiled state and their size distribution is stationary. In contrast, for $Wi > 1/2$ stretching proceeds in time until the finite extensibility limit is reached or turbulence stops the growth of dumbbells. This transition at $Wi \simeq 1/2$ is known as the coil-stretch transition. [33] The properties of such a transition in random and short-in-time correlated flows have been studied analytically. [17, 18, 19, 20] The probability density function (PDF) of end-to-end distance $R = |\mathbf{R}|$ exhibits then algebraic tails for $Wi < 1/2$, i.e. when $R \rightarrow \infty$ one gets a scaling law $P(R) \sim R^{-1-q}$ where q depends linearly on Wi^{-1} . In case of Hookean dumbbells, the PDF is not any longer normalizable at values $Wi > 1/2$.

Although the analytical treatment is possible only for this limited class of random short-correlated flows, the coil-stretch transition appears in other turbulent flows. Experimental [7, 15] and several numerical studies [9, 13, 19, 34, 35, 36, 37] all provide direct or indirect verifications of such a transition within different models for polymers or in distinct flow geometries. A sharp transition from a preferentially coiled to a preferentially stretched state at $Wi = Wi_c$ is however often not observable since different local flow topologies cause differently large mean extensions, as known from single molecule experiments. [10, 11]

III. STRETCHING PROPERTIES OF THE SHEAR FLOW

Let us discuss now the stretching properties of the shear flow. The dependence of the Lyapunov spectrum on the shear rate S is shown in upper panel of Fig. 3. One can see that all three exponents grow monotonically in magnitude with increasing S . The lower panel of the same figure shows the largest Lyapunov exponent as a function of the Taylor microscale Reynolds number R_λ . Furthermore, the strength of the shear can be quantified by the dimensionless shear

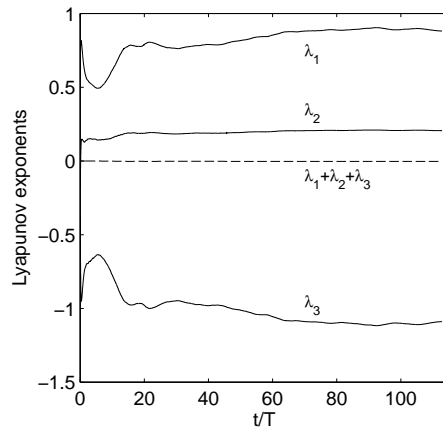


FIG. 2: Time evolution of the three Lyapunov exponents λ_i for the simulation with a shear rate $S = 7/\pi$. The dashed line is the sum of the exponents which has to be zero due to incompressibility of the flow. Time is in units of the large scale eddy turnover time $T = \langle v^2 \rangle / (2\langle \epsilon \rangle)$. 1000 Lagrangian tracer particles were seeded homogeneously at the beginning of the simulation.

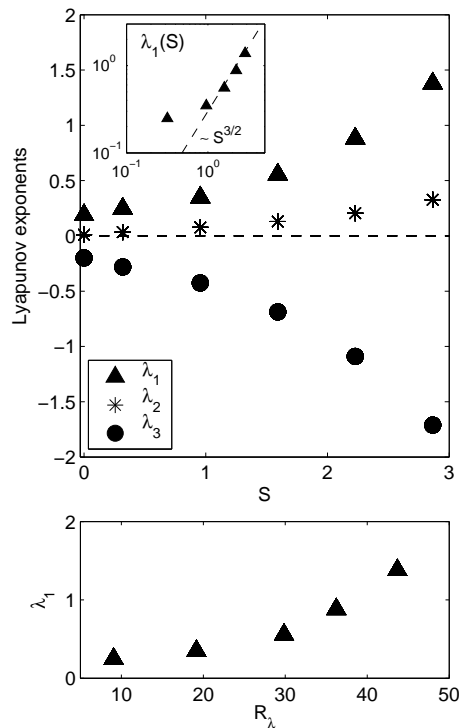


FIG. 3: Upper panel: Lyapunov spectrum λ_i for $i = 1, 2, 3$ as a function of shear rate S . The inset replots $\lambda_1(S)$ in logarithmic axes and fits a power law $\lambda_1 \sim S^{3/2}$ to the larger shear rate values. Lower panel: Largest Lyapunov exponent λ_1 as a function of the Taylor microscale Reynolds number, $R_\lambda = \sqrt{5/(3\langle \epsilon \rangle \nu)} \langle v^2 \rangle$.

parameter $S^* = S \langle v^2 \rangle / \langle \epsilon \rangle$. Table 1 indicates that this parameter saturates with growing shear rate to a value of about 8 while the Reynolds number is still increasing with growing shear rate. Such a saturation of S^* is known from studies in homogenous shear flows in the stationary regime. [29, 38, 39] Our findings as given by Fig. 3 and Tab. 1 underline the dependence of all turbulence parameters on the shear rate S .

An analytic treatment has to rely on a simpler case. In Ref. 23, the fluctuating Kraichnan flow is added with a linear shear flow which gives a decomposition as in (3). The correlation matrix of the Gaussian fluctuating strain is defined as $\langle \nabla_i v_j(t) \nabla_k v_l(t') \rangle = DC_{ijkl} \delta(t - t')$. It contains an amplitude parameter D that models the strength of the small-scale fluctuations and can be varied *independently* beside the shear rate S in the linear part. The amplitude D introduces a fluctuation time scale $T_f = D^{-1}$ beside the shear time scale $T_s = S^{-1}$.

In the large shear limit, which is defined as

$$T_s = \frac{1}{S} \ll T_f = \frac{1}{D}, \quad (14)$$

the molecules are most of the time aligned with the shear. The azimuthal angle ϕ (see Fig. 1) has a nonzero average $\langle\phi\rangle \simeq (D/S)^{1/3}$ and satisfies the asymptotic power law distribution $P(\phi) \sim 1/\phi^2$ for an intermediate range of $\langle\phi\rangle \ll \phi \ll 1$. The positive Lyapunov exponent follows to $\lambda_1 \sim S\langle\phi\rangle$ and thus

$$\lambda_1 \sim S^{2/3}. \quad (15)$$

Relation (14) is known in Navier-Stokes turbulence as being close to the rapid distortion limit of a shear flow [40], when the large shear rate determines the turbulent dynamics.

There is a slight increase of λ_1 in comparison to the isotropic case for $S \leq 1$ as the inset of the Fig. 3 indicates. However, as the shear rate increases further we observe a crossover to a faster nonlinear increase with S . In fact $\lambda_1 \sim \sqrt{\langle\epsilon\rangle}/\nu$ and $\langle\epsilon\rangle \sim S^3 L^2$ leads to the 3/2 scaling,

$$\lambda_1 \sim S^{3/2}, \quad (16)$$

which differs from (15). Although the range of our shear rates is limited, the observed scaling is consistent with this dimensional estimate. This argument and the saturation of the dimensionless shear parameter suggest that our shear flow operates in a different regime. Let us therefore compare shear and fluctuation time scale in the present case. The small-scale gradient fluctuations are captured by the Kolmogorov time $\tau_\eta = \sqrt{\nu/\langle\epsilon\rangle}$. T_s has to be related to τ_η which is known as the Corrsin parameter.[41] Figure 4 shows that

$$T_s \gtrsim \tau_\eta = \sqrt{\frac{\nu}{\langle\epsilon\rangle}} \text{ or } S\tau_\eta \lesssim 1. \quad (17)$$

In fact (16) dictates $S\tau_\eta \sim S^{-1/2}$. In order to support this behavior we add Tab. 2 where data from DNS at higher Reynolds number [29] and from turbulent boundary layer measurements [42, 43] are shown. The experimental data demonstrate that even close to the wall the Corrsin parameter does not exceed unity as can be seen for the data at $y^+ = 34$. We conclude that our studies of the polymer dynamics in the turbulent shear flow cannot be compared with the analytic results of Chertkov *et al.* [23]

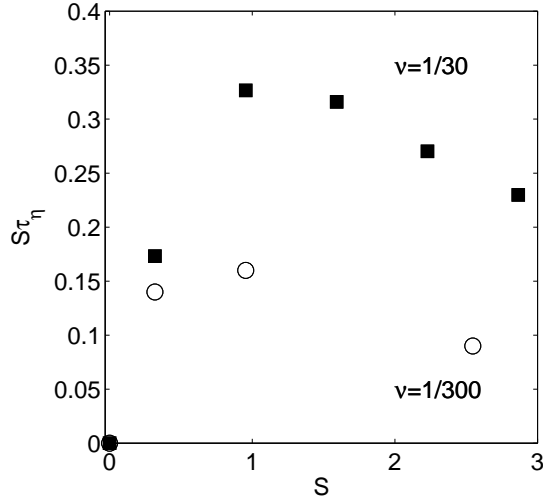


FIG. 4: Ratio of the fluctuation time scale to the shear time scale, $S\tau_\eta$. Present data are filled symbols and the open symbols are taken from Ref. 29 (see also Tab. 2).

IV. POLYMER STRETCHING

A. Statistics of dumbbell extension

Let us turn now to the stretching of the dumbbells in the described turbulent shear flow. All parameters of the runs in Brownian dynamics are summarized in Tab. 3. The corresponding turbulence parameters are as in Tab. 1.

	ν	S	y^+	R_λ	S^*	$S\tau_\eta$
DNS1	1/300	1/π	-	55	4.2	0.14
DNS2	1/300	3/π	-	175	7.7	0.16
DNS3	1/300	8/π	-	309	9.8	0.09
HFI1	ν_{air}	1576	34	151	37.8	0.97
HFI2	ν_{air}	20	1549	75	2.8	0.14
DNW1	ν_{air}	1447	709	1156	50.3	0.17
DNW2	ν_{air}	151	7826	1739	20.7	0.05
DNW3	ν_{air}	78	22753	1299	14.3	0.04

TABLE II: Further data on the ratio $S\tau_\eta$ taken from Ref. 29 (see series II in Tab. 1 there). In addition, data for two boundary layer measurements are listed. Measurements were done by Knobloch and Fernholz at the Hermann-Föttinger Institute (HFI) and the German-Dutch Windtunnel (DNW) (for more details on the experiment, see Ref. 42). The current values listed here are calculated from a data analysis by Jachens.[43] The free-stream velocity for HFI is $U_\infty = 10$ m/s and for DNW $U_\infty = 80$ m/s. For the experiments, the shear rate is given in 1/s and the kinematic viscosity of air is $\nu_{air} = 1.5 \times 10^{-5}$ m²/s.

	S	Wi	N	N_d	η/R_0	R_0/Δ
run 2p	1/π	0.26	512	2×10^6	5.5	2.0
run 3p	3/π	0.36	512	2×10^6	4.4	2.0
run 4p	5/π	0.59	128	5×10^5	1.7	1.0
run 4p1	5/π	0.26	128	5×10^5	3.4	0.5
run 4p2	5/π	0.26	128	5×10^5	1.7	1.0

TABLE III: Parameters for the shear flow simulations with the dumbbell ensemble. Other parameters of the simulations are as in Table 1. N_d is the number of dumbbells and N the grid points in streamwise direction which corresponds to a resolution of $N_x \times N_y \times N_z = N \times (N/2 + 1) \times N$. We also list the ratio of the viscous Kolmogorov scale to the equilibrium extension of the dumbbells and the ratio of the equilibrium extension to the grid spacing. The grid spacing is $\Delta = 2\pi/N$.

According to Eq. (16), effects of mean shear will enter the Weissenberg number as well. A series of three simulations (2p, 3p, 4p) is conducted for which τ is kept fixed and the Weissenberg number changes in correspondance with $\lambda_1(S)$ as shown in the upper panel of Fig. 3. In addition, runs 4p1 and 4p2 are at $Wi = 0.26$ equal to that of run 2p, but at a larger shear rate of $S = 5/\pi$. This series will demonstrate in brief another possibility of changing the physical parameters, namely keeping S fixed and varying Wi via the relaxation time τ . Furthermore, we will study the R_0 dependence of the extension statistics. Our focus anyhow will be on the first series.

In Fig. 5, we plot the instantaneous snapshot of all the dumbbells that are stretched beyond 10η for the shear rate $S = 5/\pi$ (run 4p2). A first glance on the plot indicates no preferential orientation of the polymers and a rather complicated pattern in which they are arranged. This is exactly our motivation for a more detailed study of the angular statistics which will follow at the end of this section.

First, we analyze the statistics of the end-to-end norm R . Similar to isotropic flows we detect the occurrence of the coil-stretch transition. The numerical computation of the probability density function (PDF) $p(R, t)$ for $Wi < Wi_c = 1/2$ and $Wi > Wi_c$ is shown in Fig. 6 and Fig. 7 respectively. Note that the definition of the probability density function is chosen such that $\int_0^\infty p(R, t) dR = 1$. Runs 2p, 3p and 4p2 correspond to the preferentially coiled state of the dumbbells, i.e. $Wi < 1/2$. The PDFs are stationary after a relaxation time that increases with Wi and display fatter tails with increasing shear rate S . The dependence on the equilibrium extension R_0 is shown in the inset of Fig. 6. We find that the PDF remains unchanged, except the very far tails. For both cases, R_0 was taken well inside the regular and smooth viscous range of scales of the flow which makes our finding plausible.

Run 4p corresponds with the preferentially stretched case for $Wi > Wi_c$. We plot a sequence of PDFs each taken at the times indicated in the legend of Fig. 7. Although the small scale stretching is on average dominating the Hookean spring force the PDF $p(R)$ reaches a stationary state. One may loosely think of a mean field picture that the relative velocity between the beads scales as $\Delta \mathbf{u}(R) \simeq \lambda_1 R$. Therefore under the condition that $\lambda_1 R \gtrsim R/(2\tau)$, i.e. when the Weissenberg number is larger 1/2, the average inter-bead distance should grow with time.

As mentioned in the introduction, we determine the relative velocity between the beads by taking the *full* increment between the individual bead velocities. Consequently, the dumbbells get stretched ultimately to scales $R \gtrsim \eta$ for

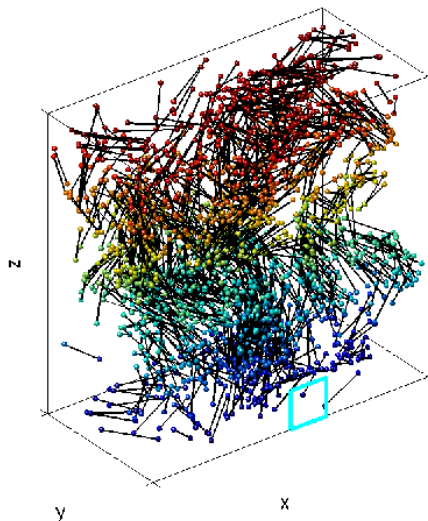


FIG. 5: (color online) Instantaneous snapshot of the dumbbell distribution in the turbulent shear flow at $S = 5/\pi$ and $Wi = 0.26$ (run 4p2). Only the dumbbells with $R \geq 10\eta$ are plotted. The scale 10η is the sidelength of the square on the bottom of the frontside of the box.

$Wi > 1/2$. At those scales the relative velocity between the beads scales as $\Delta\mathbf{u}(R) \sim R^\alpha$ with $0 < \alpha < 1$. Hence the growth of separation stops as the stretching term becomes subdominant in comparison to linear relaxation by the spring force. We add two external scales of our system into the figure. The integral scale of turbulence L_{int} (see Ref. 29 for definition) marks the average extension of the largest structures in the shear flow and therefore the end of the inertial range. The box size L_x is also shown. It can be observed that the sudden drop in the slope of $p(R)$ for later times takes place at $R < L_x$, but at $R > L_{int}$. Note that the turbulent motion is completely decorrelated across scales $R > L_{int}$ and that large extensions (which go even beyond $R = L_x$) become more and more improbable.

Such a scenario is not new, it is a main ingredient of the cascade model of drag reduction in bulk turbulence suggested by Tabor and De Gennes.[27] For a well established cascade with $\Delta\mathbf{u}(R) \simeq (\langle\epsilon\rangle R)^{1/3}$ a saturation scale of $R_* \simeq Wi^{3/2}\eta$ would follow. The mean extension $\langle R \rangle$ for the later plots of Fig. 7 is found to be at about 3η , i.e. the saturation takes place on average beyond the viscous scale of turbulence. In our case, the saturation is a result of the nonlinear advection term in Eq. (4) in combination with the Hookean spring force.

B. Anisotropy of stretching

It is important to observe that the effect of shear cannot be merely translated to an effective scaling of the Weissenberg number. The shear flow is not isotropic and hence the stretching shall not be so. To track the impact of shear we have plotted in Fig. 8 the PDFs of the individual components R_i for two cases below $Wi = 1/2$. As expected, the stretching in the streamwise direction becomes dominant when the Weissenberg number increases. The extension in y direction is always bounded to L_y due to the free slip boundary conditions. This effect is also existing for very low shear rates.

Figure 9 shows the second order moments $\langle R_i R_j \rangle$ for run 3p at $Wi = 0.36$. Effects of anisotropy are well detectable in the figure. The moment $\langle R_x R_y \rangle$ has a finite positive value while the other two mixed moments were found to vary around zero. Moreover, the moments $\langle R_x^2 \rangle$, $\langle R_y^2 \rangle$ and $\langle R_z^2 \rangle$ are no longer collapsing as for a lower shear rate. The stretching in the streamwise direction gives not only the largest extensions, but also the largest fluctuations. When comparing it with a graph of the turbulent kinetic energy of the corresponding run 3p (see inset of Fig. 9), we recognize similar patterns of time variation. They indicate that the large scale variations of the turbulence fluctuations have an effect on the stretching history, most dominantly in streamwise x -direction. For that reason we have to take statistical averages over longer time intervals with increasing S .

Such fluctuations are known for homogeneous and nearly homogeneous shear flows. We recall that the scale of variation of the mean velocity gradient is outside the considered simulation domain. Simulations which start with isotropic initial conditions will show a self-similar growth of integral scale and turbulent kinetic energy until length scales of the finite simulation domain are reached. A statistically stationary regime is then accompanied by fluctuations of the turbulent kinetic energy. [29, 38, 39] Such velocity (and kinetic energy) fluctuations show up as streamwise

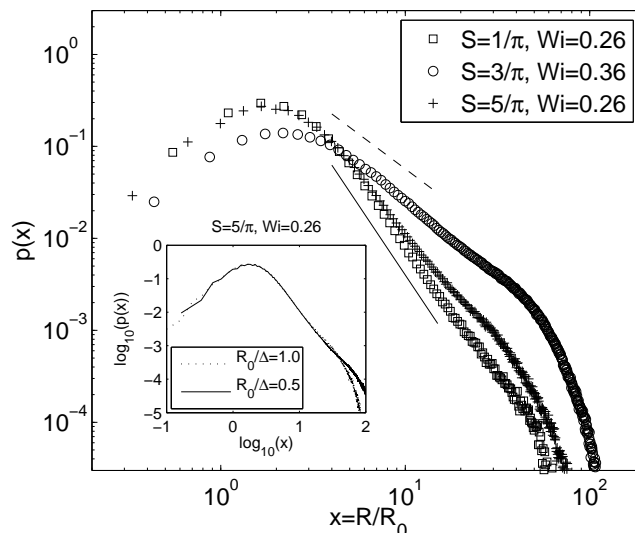


FIG. 6: Probability density function (PDF) of the dumbbell extension R as a function of the shear rate S . The length $R = |\mathbf{R}|$ is rescaled by the corresponding equilibrium extension R_0 of the advecting shear flow. Symbols are indicated in the legend. The slopes fitted to the tails are -3.0 for run 2p at $Wi = 0.26$ (solid line) and -1.5 for run 3p at $Wi = 0.36$ (dashed line). Run 4p2 at $S = 5/\pi$ and $Wi = 0.26$ is also shown in the main figure (see Tab. 3). Inset: R_0 dependence of the PDF of dumbbell extension for two different equilibrium length values as indicated in the legend (see also Tab. 3).

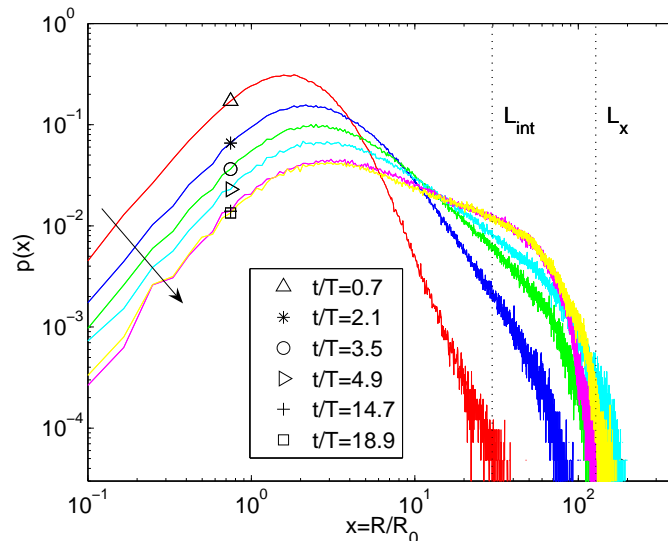


FIG. 7: (color online) PDF of the dumbbell extension for the stretching at $S = 5/\pi$ and $Wi = 0.59$ (run 4p). The extension R is rescaled again by the corresponding equilibrium extension R_0 . Curves at several times are plotted as indicated in the legend. The inclined arrow to the left indicates growth in time. $T = \langle v^2 \rangle / (2\langle \epsilon \rangle)$ is the large scale eddy turnover time. The vertical dotted lines are for the integral scale of turbulence L_{int} and the box size $L_x = 2\pi$.

streaks in the shear flow. Our studies are also in agreement with recent works by Stone and Graham[13] and Terrapon *et al.*[9] who found preferential stretching near streamwise streaks. Both cases considered a so-called minimal flow unit that captures important features of a turbulent buffer layer. In the latter work such preferential stretching study was detected by an eigenvalue analysis of the local velocity gradient along the dumbbell tracks. The streaks decay due to linear instabilities and become less coherent when the Reynolds number increases. [44] We expect that such pronounced variations in the streamwise extensions will decrease for larger Reynolds numbers.

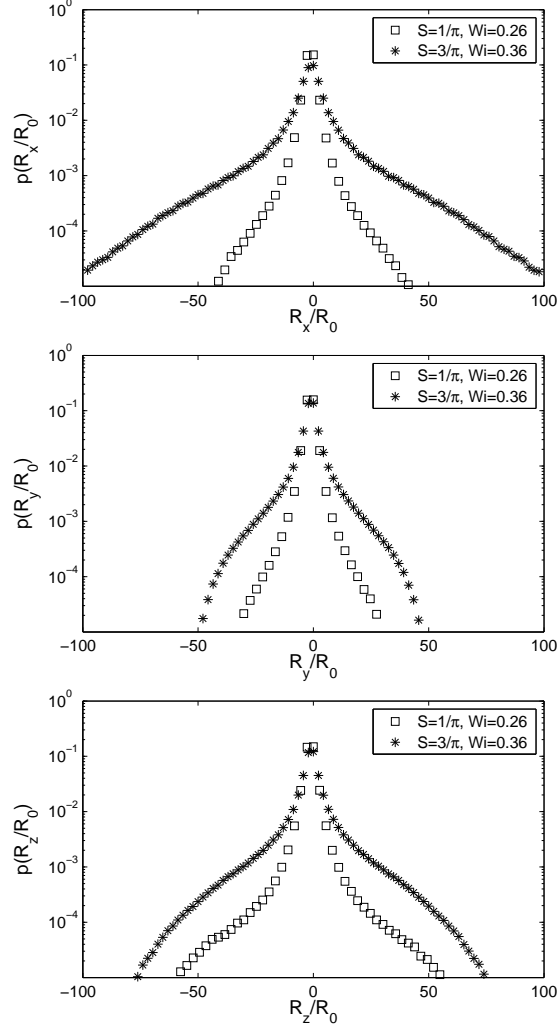


FIG. 8: Anisotropy of the stretching as quantified by the PDFs $p(R_i/R_0)$ for the streamwise component $i = x$ (upper panel), the shear component $i = y$ (mid panel), and the spanwise component $i = z$ (lower panel).

C. Angular statistics

The results of the last chapter suggest an investigation of the statistics of the azimuthal angle ϕ which measures the orientation of the dumbbells with respect to the mean flow component. The azimuthal angle is calculated as (see also Fig. 1)

$$\phi = \arctan\left(\frac{R_y}{R_x}\right), \quad (18)$$

with values between $-\pi/2$ and $\pi/2$. Figures 10 and 11 show our analysis for the runs 2p, 3p and 4p (see also Tab. 3). To resolve the anisotropy of stretching, the contour plot of the joint PDFs of extension and azimuthal angle, $p(R, \phi)$, is numerically computed and plotted in Fig. 10. They are normalized such that $\int_0^\infty dR \int_{-\pi/2}^{+\pi/2} d\phi p(R, \phi) = 1$. The lowest shear rate at $S = 1/\pi$ shows practically no variation with respect to ϕ (see upper panel of Fig. 10). For highly stretched dumbbells the ϕ probability distribution is essentially flat for almost all ϕ values except a narrow region around $\phi \simeq 0$. However this tendency of alignment with the mean flow is very weak and only visible for the most extended polymers. The dumbbell dynamics is very similar to that of an isotropic flow.

The picture changes in case of higher shear rates as can be seen in the lower panel of Fig. 10. We observe a larger number of dumbbells aligned around the mean flow axis at $\phi = 0$ even when they are not very extended. Furthermore, in comparison with lower shear, it is less probable to observe dumbbells perpendicular to x -axis, i.e. at $\phi = \pm\pi/2$.

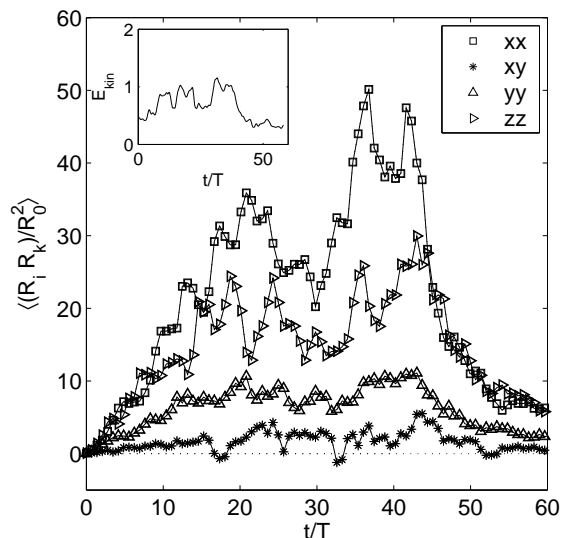


FIG. 9: Time evolution of the polymer conformation tensor components as quantified by $\langle R_i R_k \rangle / R_0^2$. Data are for $S = 3/\pi$ and $Wi = 0.36$. The symbols of the four components are given in the legend. Times are rescaled by the large scale eddy turnover time $T = \langle v^2 \rangle / (2\langle \epsilon \rangle)$. Inset: Turbulent kinetic energy as a function of dimensionless time t/T . The long time analysis was conducted at $N = 128$.

A closer inspection of both plots unravels an asymmetry in ϕ probability distribution. Dumbbells with $\phi \in [-\pi/2, 0]$ are unstable with respect to the mean flow in contrast to those with $\phi \in [0, \pi/2]$.

The PDF of the azimuthal angle is calculated by integration of the joint PDF

$$p(\phi) = \int_0^\infty dR p(R, \phi). \quad (19)$$

The angular distribution is shown in the upper panel of Fig. 11. The asymmetry between both quadrants is quantified by the following measure

$$A(\phi) = p(\phi) - p(-\phi), \quad (20)$$

with $\phi \in [0, \pi/2]$. The measure $A(\phi)$ is plotted in the lower panel of Fig. 11. Note that the integral of $A(\phi)$ determines the *total* asymmetry of the PDFs. We find that with increasing shear rate the asymmetry of the angular distribution grows. The plot of $p(\phi)$ shows a growing peak around $\phi = 0$ with increasing Wi . Fluctuations in the vicinity of $\phi = 0$ are enhanced while the tails for very large ϕ are depleted.

The second angular degree of freedom is the polar angle defined as,

$$\theta = \arctan \left(\frac{R_z}{\sqrt{R_x^2 + R_y^2}} \right), \quad (21)$$

where $\theta \in [-\pi/2, \pi/2]$. The statistics of θ is therefore reconstructed by having the full information of the three components R_i . The simultaneous statistical information of end-to-end norm R and the polar angle θ is expressed by the joint probability distribution $p(R, \theta)$ which is normalized as $\int_0^\infty dR \int_{-\pi/2}^{+\pi/2} d\theta p(R, \theta) = 1$.

Figure 12 shows the contour plots of the joint distribution $p(R, \theta)$ for runs 2p and 3p. Now, $\theta \in [0, \pi/2]$ because the dynamics is invariant under the transformation $\theta \rightarrow -\theta$ (which we verified in our simulations). The probability distribution of R at a fixed polar angle is given by vertical cuts in the two-parameter plane. For $S = 1/\pi$ (upper panel of Fig. 12), the contour levels in the vertical direction are very close and insensitive to the polar angle. A low Weissenberg number at this shear rate is consistent with close spacing of the contours in R direction and indicates a rapid decrease of the extension probability. Moreover, the decay of $p(R, \theta)$ with R at fixed θ is more or less similar for the majority of polar directions. Recall that a larger polar angle θ means that dumbbells are less aligned with the x - y shear plane. Consequently, orientations aligned with the shear plane and off that plane are equally probable. For $S = 3/\pi$ (lower panel of Fig. 12), the contour level spacing in the R direction is larger, obviously a result of the

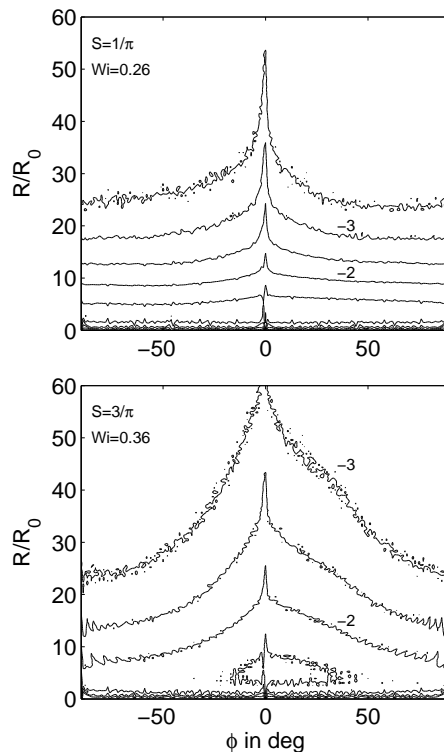


FIG. 10: Joint probability density function $p(R/R_0, \phi)$ for two different simulations. The contour levels of $p(R/R_0, \phi)$ are given in units of the decadic logarithm and decrease in steps of 0.5. Upper panel: data are for run 2p with a shear rate $S = 1/\pi$ and $Wi = 0.26$. Lower panel: data are for run 3p with a shear rate $S = 3/\pi$ and $Wi = 0.36$. The contour lines for 10^{-3} and 10^{-2} are indicated by exponents -3 and -2, respectively.

increase of Weissenberg number. The other feature is that the projected distributions along the R direction decrease more rapidly with increasing the polar angle θ . This manifests the increase of the anisotropy in θ direction. Therefore the dumbbells aligned with x - y shear plane are highly stretched only.

To demonstrate this effect, an instantaneous snapshot of the most extended dumbbells for run 4p2 is shown in Fig. 13. Again, dumbbells with $R \geq 10\eta$ are plotted only, but now in two different sectors of the polar angle. A preferential alignment of the dumbbells with smaller polar angles - sector $0 \leq \theta \leq 3\pi/20$ is compared with sector $7\pi/20 \leq \theta \leq \pi/2$ - can be clearly detected from both panels (see also Fig. 5).

Figure 14 shows the probability distribution of polar angle,

$$p(\theta) = \int_0^\infty dR p(R, \theta). \quad (22)$$

The comparison of run 4p with runs 2p and 3p shows that the number of dumbbells aligned with the x - y plane increases with shear rate. This is reflected in the increasing maximum of the probability distribution around $\theta \approx 0$.

V. SUMMARY AND DISCUSSION

We present numerical studies of the stretching of Hookean dumbbells in turbulent flows with different mean shear rates which are described by the Navier-Stokes dynamics. The flow at hand is the simplest statistically stationary turbulent shear flow, a nearly homogeneous shear flow with a linear mean profile. It can be thought as the flow in the bulk of a turbulent shear flow with no-slip boundaries, e.g. in a turbulent plane Couette flow. Beside the turbulence structures above the Kolmogorov scale η , the dumbbell dynamics around their equilibrium distance $R_0 < \eta$ is well resolved. The latter is important for the lower Weissenberg numbers where the majority of dumbbells remain below the viscous scale. This constraint clearly limits the accessible range of Reynolds numbers.

In the first part, we studied the stretching properties of the flow that are quantified by the largest finite-time Lyapunov exponent. For larger values of S our results infer that $\lambda_1 \sim S^{3/2}$ which is consistent with a simple

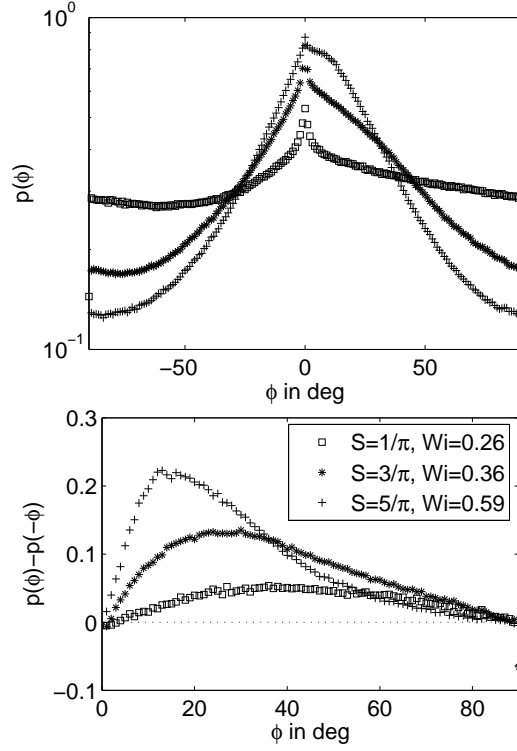


FIG. 11: Upper panel: probability density function $p(\phi)$ for the three runs 2p, 3p, 4p as given in Tab. 3. Lower panel: Corresponding asymmetry of $p(\phi)$ as given by relation (20).

dimensional analysis. Our studies and further supplementary data from other shear flows show that the Corrsin parameter does not get much larger than unity (in fact our data are all below 1). This point is important since it determines which flow time scale has to be compared with the relaxation time of the polymer chains. In our study the relevant time scale is $\sim \tau_\eta$, in contrast to S^{-1} as in a recent analytical model.[23]

In the second part of the work, we studied the shear rate dependence of the stretching properties of Hookean dumbbells. The growth of anisotropy with shear rate is quantified by measuring the statistics of R_i , the azimuthal angle ϕ , and the polar angle θ . When S grows a preferential orientation at azimuthal angles that are slightly larger than $\phi = 0$ is observed. Moreover the probability distribution of the polar angle shows a preference for smaller values of θ with increasing the shear rate. Therefore more polymers align with the shear plane as the shear rate gets higher. When keeping the shear rate fixed, the alignment of the dumbbells with the shear direction depends on the magnitude of the relaxation time τ . For higher Weissenberg numbers and therefore larger relaxation times a more pronounced anisotropic stretching is then observed. Furthermore, the $p(R)$ is found to be insensitive with respect to a variation of the equilibrium length R_0 for most extension scales.

Streamwise streaks which are a characteristic feature of shear flows are found to cause variations in the polymer extension fluctuations. In agreement with previous studies for the case of a minimal flow unit of a turbulent boundary layer[9, 13], these structures are found to enhance the stretching. For $Wi > 1/2$ the Hookean potential the inter-bead separations extend to the spatial scales where they experience a rough relative velocity difference. Therefore we detect a saturation of the stretching, even for Weissenberg numbers beyond 1/2 and in agreement with cascade models for drag reduction in the bulk of turbulence.[27]

It will be interesting to investigate the behavior of finitely extensible nonlinearly elastic (FENE) dumbbells in our flow configuration. A further parameter, the maximum length L_0 of the dumbbells, will have then an impact on the results. In that case well resolved velocity data below the Kolmogorov scale become very important. This is due to the fact that even for the largest polymer chains in turbulent flows $L_0 \lesssim \eta$. These studies are part of our future work.

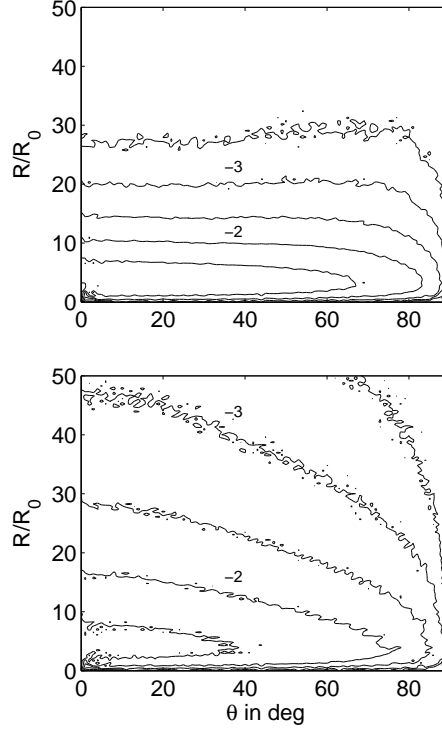


FIG. 12: Joint probability density function $p(R/R_0, \theta)$ for two different simulations. Data and line spacing are the same as for Fig. 10. Exponents for levels 10^{-3} and 10^{-2} are indicated again.

Acknowledgments

The work is supported by the Deutsche Forschungsgemeinschaft (DFG) within the Interdisciplinary Turbulence Initiative and by the German Academic Exchange Service (DAAD) within the PROCOPE program. J.S. wishes to acknowledge partial support by the NSF and thanks E. Bodenschatz for his hospitality at Cornell University where parts of this work were done. Discussions with J. Bec, E. Bodenschatz, A. Celani, L. R. Collins, C. R. Doering, B. Dünweg, B. Eckhardt, X. Hu, N. Ouellette, A. Puliafito, K. R. Sreenivasan and D. Vincenzi are acknowledged. The computations were carried out on the IBM JUMP Cluster at the John von Neumann-Institute for Computing of the Research Center Jülich (Germany). We want to thank for their steady support with computing resources.

-
- [1] J. L. Lumley, “Drag reduction by additives,” *Annu. Rev. Fluid Mech.* **1**, 367 (1969).
 - [2] P. S. Virk, “Drag reduction fundamentals,” *AIChE J.* **21**, 625 (1975).
 - [3] B. A. Toms, “Observations on the flow of linear polymer solutions through straight tubes at large Reynolds numbers,” in *Proceedings of the International Congress on Rheology (Holland 1948)*, Vol. 2, pp. 135-141 North-Holland, Amsterdam (1949).
 - [4] M. D. Warholic, H. Massah, and T. J. Hanratty, “Influence of drag-reducing polymers on turbulence: effects of Reynolds number, concentration and mixing,” *Exp. Fluids* **27**, 461 (1999).
 - [5] K. R. Sreenivasan and C. M. White, “The onset of drag reduction by dilute polymer additives and the maximum drag reduction asymptote,” *J. Fluid Mech.* **409**, 149 (2000).
 - [6] C. M. White, V. S. R. Somandepalli, and M. G. Mungal, “The turbulence structure of drag reduced boundary layer flow,” *Exp. Fluids* **36**, 62 (2004).
 - [7] C. Wagner, Y. Amarouchene, P. Doyle, and D. Bonn, “Turbulent Drag Reduction of polyelectrolyte (DNA) solutions: relation with the elongational viscosity,” *Europhys. Lett.* **64**, 823 (2003).
 - [8] A. Liberzon, M. Guala, B. Lüthi, and W. Kinzelbach, “Turbulence in dilute polymer solutions,” *Phys. Fluids* **17**, 031707 (2005).
 - [9] V. E. Terrapon, Y. Dubief, P. Moin, E. S. G. Shaqfeh, and S. K. Lele, “Simulated polymer stretch in a turbulent flow using Brownian dynamics,” *J. Fluid Mech.* **504** 61 (2004).

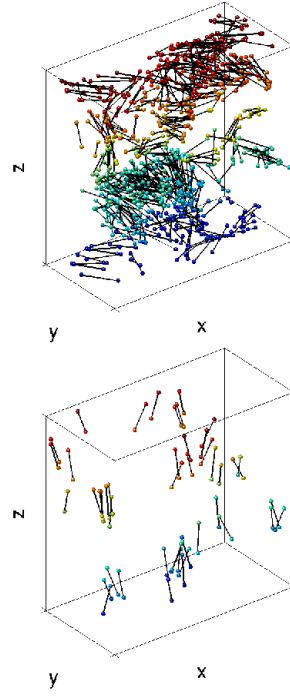


FIG. 13: (color online) Instantaneous snapshot of the dumbbell distribution in the turbulent shear flow (run 4p2). Same data as in Fig. 5 are used. Upper panel: dumbbells for $R \geq 10\eta$ and $|\theta| < 27$ degrees. Lower panel: dumbbells for $R \geq 10\eta$ and $|\theta| > 63$ degrees.

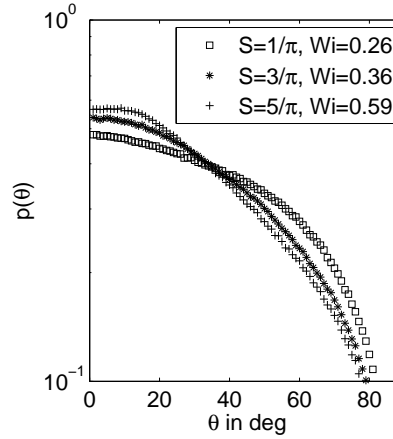


FIG. 14: Probability density function $p(\theta)$ for the three runs 2p, 3p, 4p as given in Tab. 3.

- [10] T. T. Perkins, D. E. Smith, and S. Chu, "Single-polymer dynamics in an elongational flow," *Science* **276**, 2016 (1997).
- [11] D. E. Smith, H. P. Babcock, and S. Chu, "Single-polymer dynamics in steady shear flow," *Science* **283**, 1724 (1999).
- [12] J. S. Hur, E. S. G. Shaqfeh, H. P. Babcock, D. E. Smith, and S. Chu, "Dynamics of dilute and semidilute DNA solutions in the start-up of shear flow," *J. Rheol.* **45**, 412 (2001).
- [13] P. A. Stone and M. D. Graham, "Polymer dynamics in a model of the turbulent buffer layer," *Phys. Fluids* **15**, 1247 (2003).
- [14] A. Celani, A. Puliafito, and K. Turitsyn, "Polymers in linear shear flow: a numerical study," *Europhys. Lett.* **70**, 464 (2005).
- [15] A. Groisman and V. Steinberg, "Stretching of polymers in a random three-dimensional flow," *Phys. Rev. Lett.* **86**, 934 (2001).
- [16] S. Gerashchenko, C. Chevillard, and V. Steinberg, "Single polymer dynamics: coil-stretch transition in a random flow," *Europhys. Lett.* **71** 221 (2005).
- [17] E. Balkovsky, A. Fouxon, and V. Lebedev, "Turbulent dynamics of polymer solutions," *Phys. Rev. Lett.* **84**, 4765 (2000).
- [18] J.-L. Thiffeault, "Finite extension of polymers in turbulent flow," *Phys. Lett. A* **308**, 445 (2003).

- [19] A. Celani, S. Musacchio, and D. Vincenzi, “Polymer transport in random flow,” *J. Stat. Phys.* **118**, 531 (2005).
- [20] M. Martins Afonso and D. Vincenzi, “Nonlinear elastic polymers in random flow,” *J. Fluid Mech.* **540**, 99 (2005).
- [21] R. B. Bird, R. C. Armstrong, and O. Hassager, *Dynamics of polymeric liquids*, John Wiley & Sons, New York, 1987.
- [22] C. M. Schroeder, R. E. Teixeira, E. S. G. Shaqfeh, and S. Chu, “Dynamics of DNA in the flow-gradient plane of steady shear flow: observations and simulations,” *Macromolecules* **38**, 1967 (2005).
- [23] M. Chertkov, I. Kolokolov, V. Lebedev, and K. Turitsyn, “Polymer statistics in a random flow with mean shear,” *J. Fluid Mech.* **531**, 251 (2005).
- [24] M. M. Rogers and P. Moin, “The structure of the vorticity field in homogeneous turbulent flows,” *J. Fluid Mech.* **176** 33 (1987).
- [25] J. Schumacher and B. Eckhardt, “On statistically stationary homogeneous shear turbulence,” *Europhys. Lett.* **52**, 627 (2000).
- [26] S. K. Robinson, “Coherent motions in the turbulent boundary layer,” *Ann. Rev. Fluid Mech.* **23** 601 (1991).
- [27] M. Tabor and P. G. De Gennes, “A cascade theory of drag reduction,” *Europhys. Lett.* **2**, 519 (1986).
- [28] P. K. Yeung and S. B. Pope, “An algorithm for tracking fluid particles in numerical simulations of homogeneous turbulence,” *J. Comp. Phys.* **79**, 373 (1988).
- [29] J. Schumacher, “Relation between shear parameter and Reynolds number in statistically stationary turbulent shear flows,” *Phys. Fluids* **16** 3094 (2004).
- [30] H.-C. Öttinger, *Stochastic processes in polymeric fluids*, Springer Verlag, Berlin, 1996.
- [31] G. Benettin, L. Galgani, A. Giorgilli, and J.-M. Strelcyn, “Lyapunov characteristic exponents for smooth dynamical systems and for Hamiltonian systems: a method for computing all of them. Part 2: Numerical application,” *Meccanica* **15**, 21 (1980).
- [32] S. S. Girimaji and S. B. Pope, “Material-element deformation in isotropic turbulence,” *J. Fluid Mech.* **220**, 427 (1990).
- [33] P. G. De Gennes, “Coil-stretch transition of dilute flexible polymers under ultrahigh velocity gradients,” *J. Chem. Phys.* **60**, 5030 (1974).
- [34] R. Sureshkumar, A. N. Beris, and R. A. Handler, “Direct numerical simulation of the turbulent channel flow of a polymer solution,” *Phys. Fluids* **9**, 743 (1997).
- [35] B. Eckhardt, J. Kronjäger, and J. Schumacher, “Stretching of polymers in a turbulent environment,” *Comp. Physics Comm.*, **147**, 538 (2002).
- [36] P. Ilg, E. De Angelis, I. V. Karlin, C. M. Casciola, and S. Succi, “Polymer dynamics in wall turbulent flow,” *Europhys. Lett.* **58**, 616 (2002).
- [37] T. Vaithianathan and L. R. Collins, “Numerical approach to simulating turbulent flow of a viscoelastic polymer solution,” *J. Comp. Phys.* **187**, 1 (2003).
- [38] P. Gualtieri, C. M. Casciola, R. Benzi, G. Amati, and R. Piva, “Scaling laws and intermittency in homogeneous shear flow,” *Phys. Fluids* **14**, 583 (2002).
- [39] V. Yakhot, “A simple model for self-sustained oscillations in homogeneous shear flow,” *Phys. Fluids* **15**, L17 (2003).
- [40] A. A. Townsend, *The structure of turbulent shear flow* (Cambridge University Press, Cambridge, 1980).
- [41] S. Corrsin, “Local isotropy in turbulent shear flow,” NACA RM 58 B11 (1958).
- [42] K. Knobloch and H. H. Fernholz, “Statistics, correlations and scaling in a turbulent boundary layer at $Re_{\delta_2} \leq 1.15 \times 10^6$,” IUTAM Symposium on Reynolds Number Scaling in Turbulence, Princeton 2002, Kluwer Academic Publishers, 11 (2004).
- [43] A. Jachens, “Dynamische Korrelationen und nichtnormale Verstärkung in turbulenten Scherströmungen,” PhD thesis, Physics Department, Philipps University, Marburg, Germany (2004).
- [44] J. Schumacher, “Derivative moments in stationary homogeneous shear turbulence,” *J. Fluid Mech.* **441**, 109 (2001).